УДК 543.424

ПРИБОРЫ И МЕТОДЫ КОНТРОЛЯ

ESTIMATE OF HEATING EFFECTS IN RAMAN MICROSPECTROSCOPY AND THE ACCURACY OF STOKES/ANTI-STOKES THERMOMETRY

Ralph J. Lehnert
RENISHAW GmbH, Business Division, Raman Spectroscopy
Karl-Benz-Strasse 12, D-72124 Pliezhausen, Germany
germany@renishaw.com

Поступила в редакцию 28 июля 2001 г.

Нагрев образца значительно увеличивает неопределенность условий получения спектров в Рамановской микроспектроскопии. В работе теоретически оценен максимальный рост температуры внутри образца при воздействии лазерного излучения. Результат моделирования роста температуры представлен аналитически в виде функции свойств пробы (показатель рефракции, коэффициент абсорбции, теплопроводность), мощности лазера и значения апертуры фокусирующего объектива. Показано, что достигаемая точность определения температуры по соотношению интенсивностей стоксовской и антистоксовских полос может быть оценена теоретически, что имеет большую практическую значимость. Получена функциональная зависимость, связывающая точность определения температуры образца с основными источниками экспериментальных погрешностей. Обсуждены различные практически влияющие факторы, вызывающие ухудшение теоретического отношения dT/T.

Ральф Ленерт получил образование по физике во Фрайбургском университете (Германия), защитив диплом по молекулярной динамике жидкокристаллических эластомеров. Исследовал эффект Керра для термотропныхх и лиотропных полимерных жидких кристаллов в институте макромолекулярной химии, Фрайбург.

Уже будучи доктором философии (PhD) изучал в Саутгемптонском университете (Великобритания) химию кристаллических фторированных полимеров. Совместно с сотрудниками группы полимеров и коллоидов Кэмбриджского университета (Великобритания) исследовал структурные изменения ультратонких полимерных слоев при взаимодействии жидкость/твердое тело. По контракту проводил в отраслевой лаборатории Фраунгоферовского института механики материалов (Халле, Германия) испытания по тестированию, износу и прогнозу долговечности полимерных и полупроводниковых материалов и компонентов. С 1997 года является специалистом по применению Рамановской спектроскопии и техническим консультантом фирмы Renishaw.

Область научных интересов – изучение структуры и динамики полимерных материалов с помощью механических, оптических и спектроскопических методов.

INTRODUCTION

Soon after a theory of the Raman effect had been developed that accounted for the different radiant intensities of Stokes (I_s) and the corresponding anti-Stokes (I_{as}) bands in the harmonic oscillator approximation it was proposed to derive the absolute temperature T of the probed sample volume from the ratio I_s/I_{as} using the following relationship [1-5]:

$$I_s/I_{as} = ((\nu_0 - \nu_1)/(\nu_0 + \nu_1))^4 \cdot \exp((hc\nu_1)/(kT)) \quad (1)$$

where ν_0 the absolute wavenumber of the exciting laser line, ν_1 the wavenumber of the molecular vibration giving rise to the Raman signal and h, c and k physical constants with their usual meaning.

In practice this was, for various reasons, not always found to be feasible as outlined, for example, in [2]. In this note it is attempted to estimate the extent of heating in the focal region of a typical laser micro-Raman set-up due to the intense irradiation. Ultimately an approximation for the upper limit of the temperature rise will be expressed analytically in terms of the relevant instrument parameters and

sample properties. Also addressed will be the practical aspect of determining the error dT/T of the temperature as derived from Eq. (1). The experimental uncertainty will be derived as a function of the Raman band parameters and the instrument response. Finally, some experimental difficulties involved in using Stokes/anti-Stokes ratios for thermometric purposes will be discussed.

RESULTS AND DISCUSSION

Heating effects

Modern dispersive Raman microspectrometers utilize a conventional optical microscope to direct a laser beam onto the sample and to subsequently collect the Raman signal in back-scattering geometry. Usually non-immersion objectives with a x50 or x100 magnification and a numerical aperture of 0.55 to 0.95 are used. In the focal point the $1/e$ diameter of the laser beam waist typically lies between 1 and 2 μm for a x100 objective, depending on the wavelength and the quality of the beam and collimation optics. In the geometrical limit the $1/e$-envelope can be represented by two coaxial cones with their tips joined at the objective focal point. Waveoptical deviations from this cone shape become significant in the focal region. See Fig. 1 for details.

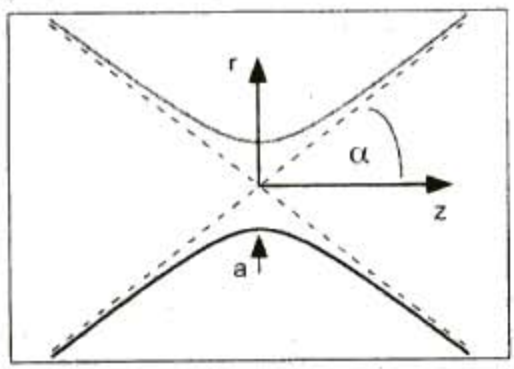

Fig. 1. Schematic cross-section of laser beam focus with the radius of the beam waist, a. Dashed lines represent envelope of laser beam in the geometrical limit. Cone half angle a is given by the objective numerical aperture and the sample refractive index. Propagation direction of laser light coincides with z-axis

Since the envelope is hyperbolic in both, the far and near focal field, the beam radius is given by $r^2 = a^2 + (a/b)^2 \cdot z^2$ where z is the distance from the focus along the cone axis while a and b are defined by $a = b \cdot \mathrm{tg}(\alpha)$ [6-10]. In air the cone half angle a can be linked directly to the objective numerical aperture by $NA = \sin(\alpha)$. The hyperboloid can be thought to consist of infinitesimally thin coaxially stacked discs of volume dV:

$$dV(z) = \pi \cdot r^2(z) \cdot dz = \pi \cdot a^2 \cdot (1 + (z/b)^2) \cdot dz \,. \qquad (2)$$

The propagating laser light passes through each disc and, in the absence of any attenuation mechanisms, the irradiance is simply the laser power divided by the disc area. The irradiance is at its maximum in the focal point where the beam diameter is smallest. This picture has to be modified if scattering and absorption effects become relevant. Subsequently it is assumed that a change of the sample refractive index with temperature is insignificant and that only absorption, in particular linear absorption, where the absorption coefficient is independent of the intensity, has to be considered. Further Lambert's law $I(dz) = I(z\text{-}z_0) = I(z_0) \cdot \exp(-A \cdot (z\text{-}z_0))$ is assumed to hold despite the non-parallel nature of the beam. The variable dz denotes the path length the light has to travel within the sample to fall ($dz>0$) by a factor of $\exp(-A \cdot dz)$ from the intensity $I(z_0)$ measured at the coordinate of the focal point, z_0. Here the directions of the z-axis and the laser propagation are chosen to be identical and z_0 was set to zero (See Fig. 1). Differentiating the so simplified relation with respect to z one arrives at the following expression for the absorbed laser energy per unit length:

$$dI(z) = -I(0) \cdot A \cdot \exp(-A \cdot z) \cdot dz \,. \qquad (3)$$

with A the absorption coefficient, $I(0)$ the laser power in and z the distance from the focus. Combining Eq.s (2) and (3) the power density of the absorbed laser energy r that eventually dissipates as heat can be expressed as follows:

$$\rho(z) = dI(z)/dV(z) = -(A \cdot I(0))/(\pi \cdot a^2) \cdot \exp(-A \cdot z)/(1+(z/b)^2) = \\ = \rho(0) \cdot \exp(-A \cdot z)/(1+(z/b)^2) \,. \qquad (4)$$

On analysing Eq. (4) it can be seen that there is exactly one local minimum as well as one local maximum "above" (towards the objective) the focal position if $A \cdot b < 1$ holds. For $A \cdot b \approx 0$ the relation simplifies to $\rho(z)/\rho(0) = 1/(1+(z/b)^2)$ representing a symmetric peak positioned at the focal point and with FWHM=2b. In this case the geometry of the beam envelope predominates the functional dependence of the power density. As $A \cdot b$ approaches 1 the minimum and maximum merge and eventually form a saddle point which transforms into a point of inflection for $A \cdot b > 1$. Representative normalised curves of the absorbed power density versus the reduced depth variable are shown in Fig. 2.

Two features in Fig. 2 are noteworthy. First, if absorption occurs and if the laser is focused within the sample, that is, the z-coordinate of the sample surface is negative, the local maximum of the power density is shifted away from the focus towards the collimation optics. This shift becomes progressively pronounced as absorption increasingly overcompen-

sates geometric effects. Second, dependent on the absorption coefficient and the distance of the focus from the sample surface the absolute maximum can be reached at the surface rather than in the focal region.

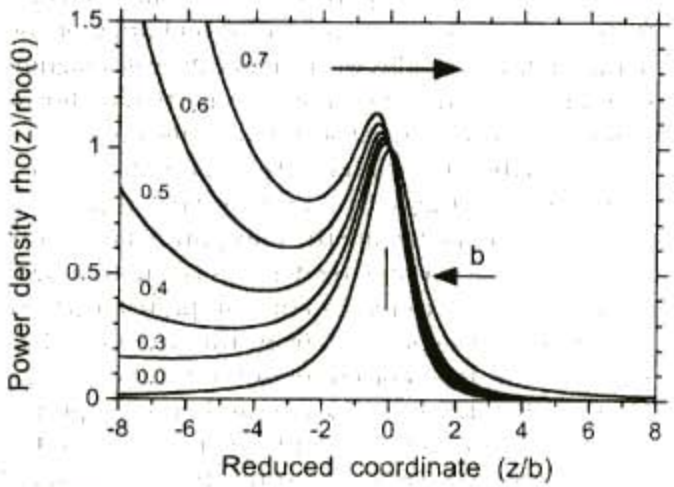

Fig. 2. Normalised power density of absorbed laser energy versus reduced z-coordinate. Curves are calculated according to Eq. (4). Annotations denote value of dimensionless factor ($A \cdot b$) with A the material absorption coefficient and b the characteristic z-length as defined in text. Upper arrow indicates propagation direction of laser light.

Instead of attempting to solve the Laplace equation for the stationary temperature field in the most general case the temperature rise will be estimated here by approximating the actual heating region by a spherical volume. As can be seen in Fig.2 for $A \cdot b \leq 0.3$ all absorbed power density curves similarly represent, in a wide z-range, a narrow heating zone around the focus which, in z, extends over a characteristic length of $2b$. The volume of this zone is $8/3\pi a^2 b$ while the radius of a sphere of equal volume is given by $R_0^3 = 2a^2 b$. Solving $\Delta T(R)=0$ in the radial coordinate R for a spherical heating zone inside an isotropic medium yields $dT(R) = T(R) - T(\infty) = P/(4\pi\lambda R)$ for the temperature elevation where P the absorbed or heating power in Watts and λ the thermal conductivity in W/(Km). Assuming the temperature gradient vanishes for $R < R_0$ inside the heating zone the maximum temperature rise becomes:

$$dT_{max} = P/(4 \cdot \pi \cdot \lambda \cdot R_0). \qquad (5)$$

The heating power can, within an error of 1.5 %, be approximated by $P = I(-b) - I(+b) = I(0) \cdot (\exp(A \cdot b) - \exp(-A \cdot b)) \approx 2 \cdot I(0) \cdot A \cdot b$ if $A \cdot b = 0.3$. Using the previous approximations and combining Eq. (5) and the expressions for R_0 and $\mathrm{tg}(\alpha)$ dT_{max} can be rewritten:

$$dT_{max} = (A \cdot I(0)/\lambda) \cdot (16 \cdot \pi^3 \cdot \mathrm{tg}^2(\alpha))^{-1/3}. \qquad (6)$$

If the focus lies inside a sample of refractive index n_s the effective cone half angle can be calculated from Snellius' law $\alpha = \arcsin(NA/n_s)$ [11] and is, like the laser power $I(0)$ in the focus, within limits, an experimentally adjustable parameter. Values for n_s range typically from 1.3 (water) to 2.4 (diamond) while the objective NA spans, for high spatial resolution work, from 0.55 to 0.95. In a simplistic approach and disregarding any refraction effects when using dry objectives [12] it can be derived from the foregoing figures that a lies between 13° and 46° and the $2b$-length of the heating zone extends over 1 to 9 μm. Hence, since the considerations assume $Ab \leq 0.3$, the upper limit for A that would be compliant with this treatment is on the order of 10^5/m. Heating is most noticeable in thermal insulators ($\lambda \approx 0.1$ W/Km) and, thus, with a laser power $I(0) \approx 1$ mW typical for micro-Raman, the first bracketed factor in Eq. (6) equals 1000 K while the second dimensionless one can vary between 0.12 and 0.34. Under these conditions a dT_{max} as large as a few hundred Kelvin is possible in principle. For poor thermal conductors ($\lambda \approx 1$ to several W/Km) this value drops accordingly. The proportionality of dT_{max} and the quotient A/λ reflects the fact that sample absorption and thermal conductivity determine equally the extent of any heating effects whereas the sample refractive index only has a small indirect influence through $\mathrm{tg}(\alpha)$ which can be offset by the choice of objective. Thus far only thermal conduction has been accounted for. Applying the Stefan-Boltzmann relation to an isolated sphere with the characteristic radius R_0 and a temperature of 700 K (room temperature plus 400 K) emitting towards a 300 K background shows that the power loss by thermal radiation is at the most a negligible 10^{-3} mW. The above considerations with respect to dT_{max} hold only in the absence of convection and are, therefore, applicable exclusively to solid matter. Also, without any resonance effects coming into play, the Raman or Rayleigh scatter cannot contribute significantly to any heating effects due to their respective weak intensities. The above figures tend to overestimate dT_{max} for several reasons the most important ones being that:

a) the heat transfer is least effective for the assumed spherical shape of the hot zone that possesses the smallest possible surface area-to-volume ratio;

b) within a sample principally unavoidable refraction effects lead to both a change of the beam profile and a substantial widening of the beam waist far in excess of the waveoptical limits.

Refraction effects are most pronounced for samples of high refractive index and dry high NA objectives and even the use of immersion liquids for

index matching can only partly compensate for them [12-14].

Accuracy of Stokes/anti-Stokes thermometry

Based on Eq. (1) the temperature of minute sample volumes, in confocal operation down to the order of femtoliters, can be determined contactless. With regard to thermometry the principally achievable temperature accuracy is of great interest and shall be assessed here. Since all modern Raman spectrometers use photon-counting detectors the intensity is measured in photon counts (C) rather than in radiant power (I). Accordingly, the radiant intensity, I_s in Eq. (1) is given by $I_s = C_s \cdot h \cdot c \cdot (\nu_0 - \nu_1)$ while an analogue expression holds for I_a. Transformation of Eq. (1) then yields the practically more relevant relation with M the relative photon count rate [3,15]:

$$M = C_s/C_a = ((\nu_0 - \nu_1)/(\nu_0 + \nu_1))^3 \cdot \exp((hc\nu_1)/(kT)). \quad (7)$$

The count rates still need to be corrected for the spectral response of the spectrometer. Usually, the finite width of the Raman bands can be disregarded and the sensitivity correction can be accomplished by applying a single factor, S to the actually measured photon count rates c_s and c_a so that $M = S c_s/c_a = C_s/C_a$. Solving now Eq. (7) for T, defining the factor $N = (\nu_0 + \nu_1)/(\nu_0 - \nu_1)$, differentiating the so obtained expression with respect to M, N and n_1 and subsequent Gauss addition of the respective absolute errors results in:

$$(dT/T)^2 = (d\nu_1/\nu_1)^2 + \\ + [\ln(M) + 3 \cdot \ln(N)]^{-2} [(dM/M)^2 + 9 \cdot (dN/N)^2]. \quad (8)$$

Assuming ν_0 and ν_1 can be measured within the same experimental uncertainty, $d\nu$ and further straightforward calculation gives $(dN/N)^2 = 4 (d\nu)^2 [(\nu_0^2 + \nu_1^2)/(\nu_0^2 - \nu_1^2)^2]$. The upper boundary for the factor in square brackets will be reached if ν_0 is at its minimum while ν_1 equals its maximum value. So the limit for $9 \cdot (dN/N)^2$ can be calculated to be less than $3 \cdot 10^{-6}$ based on $d\nu$=2 cm^{-1}, ν_0=9398 cm^{-1} (corresponding to 1064 nm NIR excitation) and ν_1=4000 cm^{-1}. This is negligible compared with the composite error $(dM/M)^2 = (dc_s/c_s)^2 + (dc_a/c_a)^2 + (dS/S)^2$ which is realistically no smaller than some $3 \cdot 10^{-4}$ because each individual error is typically at the best in the percent range. Hence Eq. (8) simplifies to:

$$(dT/T)^2 \sim (d\nu/\nu_1)^2 + (k/hc)^2 \cdot (T/\nu_1)^2 \cdot (dM/M)^2. \quad (9)$$

For a given sample temperature the weighting factor of $(dM/M)^2$ in Eq. (9) and generally also dT/T is smallest for great Raman shifts. In representative circumstances ($d\nu/\nu_1 = 1/3500$, T = 300 K and dM/M = 3 %) the best accurracy theoretically achievable is approximately 0.02 %. At the other extreme ($d\nu/\nu_1 = 1/100$, T = 1500 K, dM/M = 3 %) the value for dT/T reaches 31 % rendering any measurement effectively meaningless. In this case a Raman peak shift of 3500 cm^{-1} would reduce the error to an excellent 0.9 % again. Figures for dT/T for selected values of ν_1 and T are shown in Table.

Theoretical values for dT/T in percent for selected Raman peak shifts and sample temperatures. Calculations according to Eq. (9) assume dM/M = 3 % and $d\nu$ = 1 cm^{-1}. According to Eq. (10) dT/T is, to a first approximation, proportional to dM/M

Raman shift ν_1 [cm^{-1}]	200 K	300 K	600 K	1500 K
100	4.3	6.4	12.6	31.5
500	0.9	1.3	2.5	6.3
1500	0.3	0.4	0.8	2.1
3500	0.1	0.2	0.4	0.9

According to Eq. (10) dT/T is, to a first approximation, proportional to dM/M. For $T \cdot (dM/M) >> 1$ Kelvin and $d\nu$ = 1 cm^{-1} the second summand predominates Eq. (9) which can then be further reduced to:

$$dT/T \approx (kT)/(hc\nu_1) \cdot (dM/M) \approx \\ \approx 0.7 \text{ cm}^{-1}/\text{Kelvin} \cdot (T/\nu_1) \cdot (dM/M). \quad (10)$$

In practice, various effects additionally deteriorate dT/T. These can be classified according to whether Eq. (1) as such fails or whether the actual relative band intensities are somehow altered. Recently it was demonstrated that non-fundamental bands that owe their entire intensity to anharmonicity can show drastic deviations of their Stokes/anti-Stokes ratio from theory [16] while anharmonicity effects are commonly small for fundamentals and, therefore, with respect to inten-sity, are normally insignificant to these. Also if reso-nance effects are present the prerequisites for deriving Eq. (1) are no longer valid. Further, Raman signals collected from inside a sample can suffer from frequency dependent absorption or scattering losses that potentially modify Stokes/anti-Stokes ratios. Even if absorption effects are absent pure scattering losses can be marked causing drastic changes of the relative intensity, particularly in he-terogeneous materials [17]. Still widely unacknow-ledged is the possible chromatic aberration of the collection optics which is potentially important, especially in the near infrared region. It can change intensity ratios as the sample is placed at different distances from the objective because the optimum focus of a Raman band depends on its absolute wavenumber [18]. In

samples possessing strong dispersion the solid angle under which Raman scatter can be collected from within and therefore also signal collection efficiency varies noticeably with wavelength.

SUMMARY

The laser induced temperature rise inside a sample can be estimated and expressed analytically using few simple approximations. The sample absorption coefficient, the thermal conductivity and the laser power are equally relevant parameters whereas the sample refractive index and the objective numerical aperture only have a minor influence. The notion of a hot spot located exactly at the focus position provides an increasingly inaccurate picture as absorption increases. In fact the zone of highest thermal energy density rather lies somewhere between the focus and the sample surface. On assessing the principally achievable accuracy of temperature determination by Stokes/anti-Stokes ratios it has been shown that dT/T is approximately proportional to the Gauss sum of the relative errors related to measurements of the instrument response and the two Raman band intensities. The temperature can realistically be measured within 1 % error at sufficiently high Raman shifts at the cost of long acquisition times because of the weakness of the anti-Stokes band.

REFERENCES

1. Placzeck G. Rayleigh-Streuung und Raman-Effekt // Handbuchder Radiologie/ E. Marx,Ed. Leipzig: Akademischer Verlag, 1934. Chap. VI. P.205

2. Brandmüller J., Moser H. Einführung in die Ramanspektroskopie. Darmstadt: Steinkopff Verlag, 1962. 245 p.

3. Hayes W., Loudon R. Scattering of Light by Crystals. New York: John Wiley and Sons, 1978. P. 26

4. Malyj M., Griffiths J. E. Stokes.Anti-Stokes Raman Vibrational Temperatures: Reference Materials, Standard Lamps, and Spectrophotometric Calibrations // Appl. Spectrosc. 1983. V 37, № 4. P.315.

5. Rassat S. D., Davis E. J. Temperature Measurement of Single Levitated Microparticles Using Stokes/Anti-Stokes Raman Intensity Ratios // Appl. Spectrosc. 1994. V.48, №12. P.1498.

6. Eppich B., Weber H. Beam characterization by use of the Wigner distribution//LaserOpto. 2000. V. 32, № 4. P.43.

7. Eppich B. Die Charakterisierung von Strahlungsfeldern mit der Wigner-Verteilung und deren Messung. PhD thesis. Berlin, 1998. Chap. 9. P.104.

8. Belanger P. A. Beam Propagation and the ABCD ray matrices // Optics Letters. 1991. V. 16. № 4. P.196.

9. International Standard ISO 11146. Laser and laser-related equipment – Test methods for laser beam parameters – Beam widths, divergence angle and beam propagation factor. 1999.

10. Siegmann A. E. An Introduction to Lasers and Masers. McGraw-Hill, 1971.

11. Turrell G. Raman Sampling, in Practical Raman Spectroscopy / D.J. Gardiner and P. R. Graves, Eds. Berlin Heidelberg: Springer-Verlag, 1989. Chap. 2. P.30

12. Everall N. Confocal Raman Microscopy: Why the Depth Resolution and Spatial Accuracy Can Be Much Worse than You Think//Appl. Spectrosc. 2000. V.54, N10. P.1515.

13. Baldwin K. J., Batchelder D. N. Confocal Raman Microspectroscopy through a Planar Interface // Accepted for publication in Appl. Spectrosc. in 2001.

14. Visser T. D., Oud J. L., Brakenhoff G. J. Refractive index and axial distance measurements in 3-D microscopy // Optik. 1992. V. 90, N 1. P. 17.

15. LaPlant F., Laurence G., Ben-Amotz D. Theoretical and Experimental Uncertainty in Temperature Measurement of Materials by Raman Spectroscopy // Appl. Spectrosc. 1996. V. 50, N 8. P. 1034.

16. Meier R. J., v. d. Pol A. A versatile aid in spectrum assignment: discriminating between fundamental and non-fundamental vibrational bands in Raman spectra // Vib. Spectrosc. 2000. V. 23. P.95.

17. Lehnert R. J. Studies on the crystallinity of poly(tetrafluoroethylene). PhD thesis. Southampton (UK), 1994. P.68 and P.106 .

18. Everall N., King B. Raman Spectroscopy for Polymer Characterization in an Industrial Environment // Macromol. Symp. 1999. V. 141. P.103.

* * * * *